CHARACTERISTICS OF ACTIVE MAGNETIC BEARINGS BIASED WITH PERMANENT MAGNETS ON THE ROTOR

Satoru Fukata
Department of Engineering Design, Kyushu Institute of Design
4-9-1 Shiobaru, Minami-ku, Fukuoka 815, Japan.

Kazuyuki Yutani
Graduate Student, Kyushu University
Fukuoka 812-81, Japan.

SUMMARY

An active magnetic radial bearing is constructed by a combination of permanent magnets for biasing and electromagnets for control. A ring-shaped permanent magnet with axial magnetization is arranged between two rotor cores on a shaft and shares all the pole legs with the electromagnets. The stator is composed of two rings having four pole legs in their inner side and four connecting segments giving the permanent-magnetic flux path. This composition is similar to that of a case where permanent magnets are arranged in the stator. In the non-rotating state, frequency responses of the rotor positioning control system are measured and the transient rotor-motion for impulsive force is tested. The frequency responses are compared with numerical results based on a simple model. In the rotating state, the decay of rotation due to magnetic braking with air friction is examined together with the whirling of the rotor.

INTRODUCTION

A combination of permanent magnets to give bias forces and electromagnets to generate control forces by be useful for the reduction of cost and running energy comsumption of electromagnetic bearings (refs. 1-2). Allaire *et al.* (ref. 3) reviewed work related to this subject, discussed the design and construction, and gave experimental data to show the merit. In this combined magnetic system, the permanent magnets are arranged in the stator in usual, and the stator is shared by two electromagnetic systems in the vertical and horizontal directions. Hence, the magnetic systems interact with each other in general.

In this combination, another arrangement is possible: the permanent magnet is attached to the rotor. This arrangement may have a disadvantage in practice, because there are some problems in the composition of the rotor; however, we can design less interacting magnetic systems with separated stators being homopolar in geometry. The authors (ref. 4) constructed a setup of this arrangement using solid magnet cores, for simplicity, and confirmed that the characteristics are similar to those of the all electromagnetic design. With the separated stators, however, the electromagnetic flux takes an axial path where the magnet core is difficult to laminate. Hence, the response of the electromagnet decays because of eddy current effects. Thus, this arrangement has a merit in the interaction problem but has a demerit in the dynamics. Another demerit is in the setting up of the separate stators into the frame.

To overcome the demerits of this arrangement, without giving up the merit, we consider another stator that is similar to the case of arranging the permanent magnets in the stator. Decoupling control systems are designed with analog PID compensators, neglecting the gyroscopic effect. Frequency responses of

the rotor motion to a disturbance input and the motion for an impulsive force are tested in the non-rotating state. The frequency responses are compared with the numerical results based on a simple model. In the rotating state, the decay of rotation due to magnetic braking with air friction is examined together with the whirling of the rotor.

CONSTRUCTION AND MAGNETIC SYSTEM OF RADIAL BEARINGS

Figure 1 illustrates the construction and the main flux paths of radial magnetic bearings composed of a permanent magnet for biasing and electromagnets for control. A ring-shaped permanent magnet with axial magnetization is arranged between two rotor cores on a shaft of non-ferromagnetic material. The stator is composed of two rings having four pole legs in their inner side and of four connecting segments of ferromagnetic material. The stator rings are made of laminated stacks. The permanent magnetic flux flows radially in the rotor core and goes into the pole leg through the airgap, and passes through the connecting segment to return to the rotor via the other airgap.

The electromagnet coils installed on the radially opposing pole legs are connected in series together with those of the other stator ring and are driven by a single power amplifier. The electromagnetic flux passes down or up the stator pole-leg, through the working airgap and the rotor radially, and enters the radially opposing pole leg. The return flux takes two paths along the stator ring, as shown in the figure. Thus, we can control the total flux by increasing current on one side of the rotor and decreasing current on the other side. A part of the electromagnetic flux may pass the stator axially in the same way as the permanent magnetic flux; but this quantity decreases with increasing frequency because of eddy current effects in the connecting segments that are not laminated for the flux path, in general.

The construction of the stator is similar to that of the case where biasing permanent magnets are

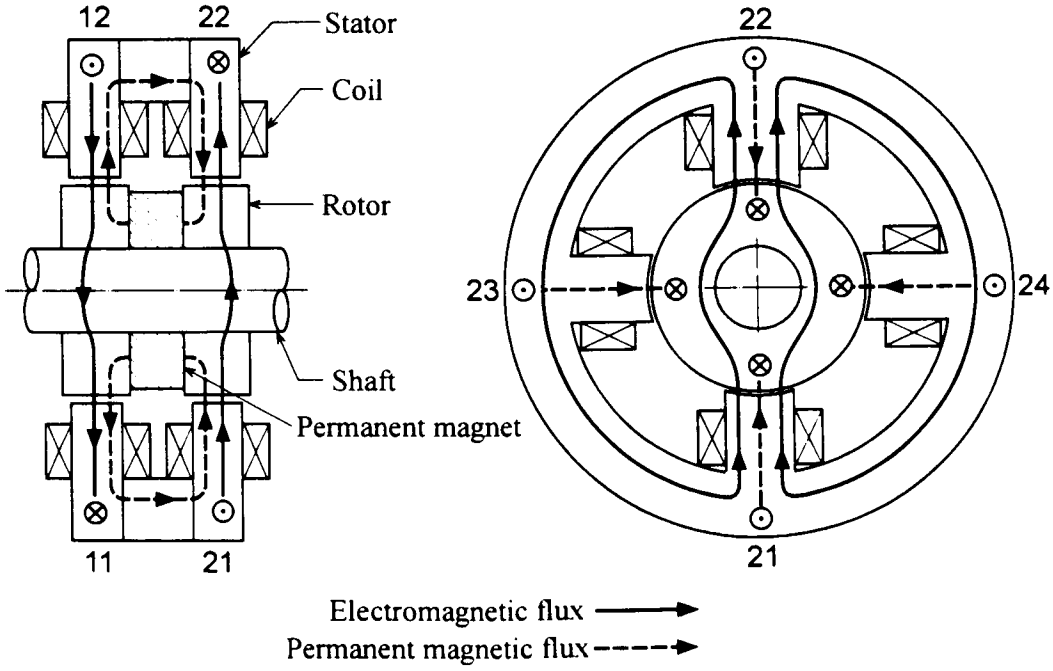

Figure 1. Construction and main flux paths of magnetic radial bearings biased with permanent magnet on the rotor.

located in the stator, where the permanent magnet segments take the place of the connecting segments. With this stator ring connecting the four pole legs, the two magnetic systems are supposed to interact with each other more than with separated stators in ref. 4; however, the response is faster because the electromagnetic flux in large part takes the path of the laminated cores.

Since the composition resembles the case of arranging the permanent magnets in the stator, the magnetic circuit model is derived in a similar way to that in ref. 5. The model may be simplified as in **Fig. 2**, where the left-hand part gives the magnetic parallel circuit of the single stator ring (each path corresponds to a single pole leg), and the right-hand is the equivalent single path of the other stator ring. The symbols F_{ij} and R_{ij} are the magnetomotive force and magnetic resistance of a single pole-leg coil system, and Φ_{ij} is the magnetic flux. The lower part is the axial path in the connecting segments between the two stator rings with the magnetic resistance R_S; the upper is the axial path in the rotor and the permanent magnet with the magnetic resistance R_R. The characteristics of the permanent magnet are considered with the imaginary magnetomotive force F_B and the magnetic internal resistance R_B. In general, since the magnet cores are difficult to laminate in the radial direction, R_S and R_R become larger with frequency because of eddy current effects. Hence, the axial electromagnetic flux may be smaller at higher frequencies.

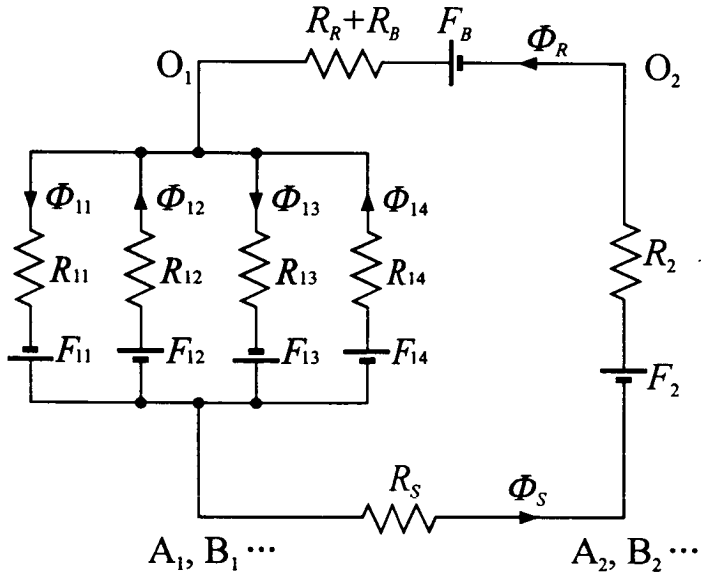

Figure 2. Simplified magnetic circuit.

A DYNAMIC MODEL OF THE MAGNETIC SYSTEM

Symbols

b_j : gain of power amplifier (ratio of output current to input voltage)
c_{Rij} : relative increment of magnetic resistance
e_j : incremental input voltage into power amplifier
I_{j0} : bias coil current

i_j : incremental coil current

$l_{mij\,0}$: equivalent airgap length considering magnetic resistance of magnet core

N_{ij} : turns of magnet coil

Q_{Bij} : equivalent permanent magnetic flux having the unit of current

$Q_{ij\,0}$: similar equivalent bias magnetic flux

q_{ij} : incremental equivalent magnetic flux

R_{ij} : magnetic resistance associated with working airgap

$R_{ij\,0}$: nominal magnetic resistance

R_R : axial magnetic resistance of rotor

R_S : axial magnetic resistance of connecting segments

$R_{T\,0}$: nominal total magnetic resistance

T_{Cj} : time constant of total electromagnet system

T_{Cij} : time constant of individual electromagnet system

T_{Rj} : time constant associated with working airgap variation

Φ_{ij} : magnetic flux associated with working airgap

$\alpha_{i0}, \alpha_{ij\,0}$: ratio between two magnetic resistances

$\Delta\alpha_{ijk}$: difference between α_{ij}

β_{ij} : gain of incremental flux to coil current

μ_0 : permeability of air ($= 4\pi \times 10^{-7}$ H/m)

τ_j : dead time of electromagnet system

We number the pole legs and the working airgaps with *ij* where $I = 1, 2$ for the left- and right-hand stator rings, respectively, $j = 1, 2$ for the lower and upper sides and $j = 3, 4$ for the left- and right-hand sides, respectively, in each stator ring (see Fig.1, for example). The magnet system is referred by 1 for the vertical direction and by 3 for the horizontal direction. These numbers will be used in the subscript to show the associated variables and constants.

Assumption

The analysis of the magnetic system is very complicated in general, as seen in ref. 5. We consider a simple case with the following conditions:

(C1) In the horizontal direction, the dimensions of the magnet system are equal in each stator ring, and

(C2) there is no bias load: no bias current in the electromagnet.

(C3) The nominal working airgap lengths are equal in each direction.

We make the following assumptions:

(A1) Rotor displacement is sufficiently small.

(A2) Incremental magnetic fluxes are sufficiently small.

(A3) Magnetic leakage resistances are constant.

(A4) The recoil permeability of the permanent magnet is equal to that of air.

(A5) Eddy-current effects in the axial flux paths are negligible.

Initial Steady-State Values

For the magnetic fluxes, we use the variables having the unit of current and giving the dynamical characteristics of the fluxes, which are defined by

$$Q_{ij} = \frac{R_{ij0}}{N_{1j}} \Phi_{ij}, \quad i = 1,2;\ j = 1 \sim 4 \tag{1}$$

We denote the initial steady-state values with subscript 0. Then, from the results in ref. 5 obtained under conditions (C1) to (C3), we have the following relations with the nominal working airgap.

$$Q_{ij0} = \beta_{ij} I_{10} + (-1)^{j-1} Q_{Bij},\ j = 1,2; \qquad Q_{i30} = -Q_{i40} = -\frac{N_{11}}{N_{13}} \gamma_{i10} I_{10} + Q_{Bi3} \tag{2}$$

where

$$\frac{1}{R_{i0}} = \sum_{j=1}^{4} \frac{1}{R_{ij0}}, \qquad R_{T0} = R_{10} + R_{20} + R_S + R_R$$

$$\alpha_{i0} = \frac{R_{i0}}{R_{T0}}, \qquad \alpha_{ij0} = \frac{R_{i0}}{R_{ij0}}$$

$$\alpha_{i12} = \frac{N_{i1}}{N_{11}} \alpha_{i10} + \frac{N_{i2}}{N_{11}} \alpha_{i20}, \qquad \Delta\alpha_{i12} = \frac{N_{i1}}{N_{11}} \alpha_{i10} - \frac{N_{i2}}{N_{11}} \alpha_{i20}$$

$$\beta_{ij} = \frac{N_{ij}}{N_{1j}} + (-1)^j \frac{N_{11}}{N_{1j}} \gamma_{i10}$$

$$\gamma_{i10} = \Delta\alpha_{i12} - \alpha_{i0}\left(\Delta\alpha_{112} + \Delta\alpha_{212}\right)$$

The above equations are formulated so that they are applicable to the cases where the right-hand stator ring has no electromagnet coil and/or the dimensions are different on the left- and right-hand sides. Hence, the constants are complicated in form, but become simpler in the case of the same dimensions on both sides. The equivalent permanent-magnetic bias current Q_{Bij} may be given with the data of the permanent magnet; but we may also obtain it directly from the measurement of the magnetic flux densities B_{ij0} by

$$Q_{Bij} = \frac{l_{mij0}}{\mu_0 N_{1j}} B_{ij0} \tag{3}$$

Incremental Magnetic Fluxes

We denote the increments by lower letters. From the results in ref. 5 obtained under assumptions (A1) to (A4), with assumption (A5) we have the following relations for the increments, for $i = 1,2$.

Vertical direction: $j = 1,2$

$$q_{ij} - Q_{ij0}' c_{Ri1} = \beta_{ij} i_1 \tag{4}$$

$$T_{C1} \dot{i}_1 + i_1 + T_{R11} \dot{c}_{R11} + T_{R21} \dot{c}_{R21} = b_1 e_1 (t - \tau_1) \tag{5}$$

Horizontal direction: $j = 3, 4$

$$q_{ij} = \bar{q}_{i3} + (-1)^j \Delta q_{i3}, \qquad \bar{q}_{i3} - Q_{i30} c_{Ri3} = \frac{N_{i3}}{N_{13}} i_3,$$

$$\Delta q_{i3} = \frac{N_{11}}{N_{13}} \left(\gamma_{i10} i_1 + \gamma_{R1i} I_{10} c_{Ri1} \right) \tag{6}$$

$$T_{C3} \dot{i}_3 + i_3 + T_{Ri3} \dot{c}_{Ri3} + T_{Ri23} \dot{c}_{Ri23} = b_3 e_3 (t - \tau_3) \tag{7}$$

where

$$c_{Rij} = \frac{R_{ij}}{R_{ij0}} - 1, \qquad Q_{ij0}' = (-1)^{j-1} \left(Q_{ij0} - \frac{N_{11}}{N_{1j}} \gamma_{R1i} I_{10} \right)$$

$$T_{C1} = \sum_{i=1,\ j=1}^{2} \beta_{ij} T_{Cij}, \qquad T_{C3} = 2 \left(T_{C13} + T_{C23} \right)$$

$$T_{Ri1} = \sum_{j=1}^{2} Q_{ij0}'\ T_{Cij}, \qquad T_{Ri3} = 2 Q_{i30} T_{Ci3}$$

$$\gamma_{R1i} = \alpha_{i12} - \alpha_{i0} \left(\alpha_{112} + \alpha_{212} \right)$$

In the equations of coil current, eqs. (5) and (7), we added time lags τ_j that may be due to the dynamical characteristics of the power amplifier.

The above model says that the magnet system in the horizontal direction is disturbed by that in the vertical direction, with the effects of the bias coil current I_{10} and the term γ_{i10} that is based on the asymmetry of a pair of electromagnets in the vertical direction. The bias current is given to suspend the rotor against the gravity and a bias load in the vertical direction; c ondition (C2) gives no bias current in the horizontal direction. The relations are complicated by γ_{i10}, but those become much simpler in the symmetric bearing, i.e., γ_{i10} =0 when the dimensions of the magnetic system are equal in the vertical direction.

Net Force in Single Stator Ring

We express the magnetic force as

$$F = \frac{A_h B^2}{2\mu_0} = \frac{A_h}{2\mu_0} \left(\frac{\Phi}{A} \right)^2 = \frac{\mu_0 A_h}{2} \left(\frac{N}{l_{m0}} \right)^2 Q^2 \tag{8}$$

where

$$Q = \frac{R_{m0}}{N} \Phi, \qquad R_{m0} = \frac{l_{m0}}{\mu_0 A}$$

and where A is the area of pole-leg face, A_h its cross-sectional area, B the magnetic flux density, N the turns of magnet coil, l_{m0} the equivalent airgap length and Φ the magnetic flux. Applying this expression to the opposing pole legs, we have the force acting on the rotor as

$$F_{i12} = c_{Fi1} \left(Q_{i1}^{\ 2} - c_{ANi} Q_{i2}^{\ 2} \right)$$

where

$$c_{Fi1} = \left[\frac{\mu_0 A_h}{2}\left(\frac{N}{l_{m0}}\right)^2\right]_{i1}, \qquad c_{ANi} = \frac{c_{Fi2}}{c_{Fi1}} = \frac{A_{hi2}}{A_{hi1}}\left(\frac{N_{i2}}{N_{i1}}\right)^2 \tag{9}$$

Then, the net force is given by

$$\Delta F_{i12} = F_{i12} - F_{i120} = f_{i1} + c_{Fi1}\left(q_{i1}{}^2 - c_{ANi}\, q_{i2}{}^2\right)$$

with the incremental force

$$f_{i1} = (k_{Fi1}/2)\left(q_{i1} + c_{Qi1} q_{i2}\right) = k_{Fi1}\bar{q}_{i1}, \qquad 2\bar{q}_{i1} = q_{i1} + c_{Qi1} q_{i2} \tag{10}$$

where

$$k_{Fi1} = 4 c_{Fi1} Q_{i10} = 4\frac{F_{i10}}{Q_{i10}}, \qquad c_{Qi1} = c_{ANi}\frac{-Q_{i20}}{Q_{i10}} = \frac{A_{hi2}}{A_{hi1}}\left(\frac{N_{i2}}{N_{i1}}\right)^2 \frac{-Q_{i20}}{Q_{i10}} \ (>0) \tag{11}$$

For $\bar{q}_{i1}$ in eq. (10), from eq. (4) we have

$$\bar{q}_{i1} - \bar{Q}_{i10}{}' c_{Ri1} = \bar{\beta}_{i1} i_1 \tag{12}$$

where

$$\bar{Q}_{i10}{}' = \frac{1}{2}\left(Q_{i10}{}' + c_{Qi1} Q_{i20}{}'\right), \qquad \bar{\beta}_{i1} = \frac{1}{2}\left(\beta_{i1} + c_{Qi1}\beta_{i2}\right)$$

With the relative increment of the magnetic resistance c_{Ri1}, we take a variable z_i as the vertical displacement of the rotor onto the lower side, positive when the rotor approaches a pole leg numbered by $i1$. Then, c_{Ri1} may be approximated by

$$c_{Ri1} \cong -\frac{z_i}{l_{mi10}} \tag{13}$$

The total incremental force of the two stator rings is given by the summation of the forces of eq. (10) with $i = 1, 2$.

LINEARIZED DYNAMICS OF RIGID-ROTOR-SUPPORTING BEARINGS WITH ELECTROMAGNETS OF EQUAL DYNAMICS

We consider a rigid rotor supported by the two radial bearings. To obtain the resultant incremental force and moment acting on the rotor in a simple form, we add the following conditions:

(C4) The two stator rings have equal dimensions with the electromagnetic system in each bearing [$A_{11} = A_{21}$, $A_{12} = A_{22}$, $N_{11} = N_{12}$, $N_{21} = N_{22}$ and $l_{m110}\,(= l_{m120}) = l_{m210}\,(= l_{m220})$].

(C5) The dynamical characteristics of the electromagnet systems are equal in each direction (vertical or horizontal) in the two bearings.

Incremental Force

We take the vertical rotor-displacement z at the center of the bearing, and we assume that the effects of the conical displacement on the magnetic resistances are negligible. In this case, from eqs.

(10), (12), (13) and (5) under condition (C4), we obtain the total incremental force of the single bearing as

$$f_1 = k_{F1} q_1, \qquad T_{C1}\dot{q}_1 + q_1 - a_{10} z = \bar{\beta}_{11} b_1 e_1 (t - \tau_1) \tag{14}$$

where

$$k_{F1} = 2k_{F11}, \qquad a_{10} = \frac{Q_{110}'}{2l_{m110}}\left(1 + c_{Q11} c_{Q11}'\right), \qquad c_{Q11}' = \frac{Q_{120}'}{Q_{110}'} \tag{15}$$

In the second of eq. (14) we have omitted a term with $\dot{z}$ by presuming that it is negligible in general. We note that the above relation is formulated with a single stator ring. This is reflected in the factor of the force.

For the horizontal direction, the disturbing term Δq_{i3} in eq. (6) is cancelled out, and the equation is given by a simple form as a special case of the above result with $\bar{\beta}_{11}$=1, $Q_{110}' = Q_{130}$, $c_{Q11} = c_{Q11}'$=1, etc. For the displacement y, we have

$$f_3 = k_{F3} q_3, \qquad T_{C3}\dot{q}_3 + q_3 - a_{30} y = b_3 e_3 (t - \tau_3) \tag{16}$$

Equations of Rigid-Rotor Motion

We number the two bearings by 1 and 2 on the left- and right-hand sides, respectively, and use these numbers in the subscript of the variables if necessary. We take the sense of the rotor displacement to be positive when going down, as in the above, and the sense of the conical motion to be positive when going down more in bearing 1 than in bearing 2. Then, neglecting the gyroscopic effects in the conical motions, we have the equations of the translatory and conical motions of rigid rotor:

$$m\ddot{z} = f_1 + f_2 + d_z, \qquad J\ddot{\theta} = L_1 f_1 - L_2 f_2 + M(d_z) \tag{17}$$

where z is the translatory displacement of the gravity center of rotor, θ the angle of the conical motion, m the rotor mass, J the moment of inertia, L_j the distance between the gravity center of rotor and the bearing center, f_j the net force in the bearing, d_z a resultant disturbing force acting on the rotor, and $M(d_z)$ the resultant moment of disturbing forces.

The variables z and θ are related with the displacements in two bearings in the rigid-rotor motion by

$$z_1 \cong z + L_1\theta, \qquad z_2 \cong z - L_2\theta$$

For the angle of the conical motion, we take the displacement defined by

$$z_C \equiv \frac{1}{2}(z_1 - z_2) \cong L\theta, \qquad L = \frac{1}{2}(L_1 + L_2) \tag{18}$$

In applying eq. (14) to the two bearings with $T_{C1} = T_{C2}$ under condition (C5), we set

$$2e_z = e_1 + c_{ez} e_2, \qquad 2e_{zC} = \frac{L_1}{L} e_1 - \frac{L_2}{L} c_{ez} e_2 \tag{19}$$

where

$$c_{ez} = c_{kFz} \frac{\bar{\beta}_{21}}{\bar{\beta}_{11}} \frac{b_2}{b_1}, \qquad c_{kFz} = \frac{k_{F2}}{k_{F1}}$$

Then, we obtain the following equations.

$$m\ddot{z} = 2k_{F1}q_z + d_z, \qquad T_{C1}\dot{q}_z + q_z - a_z z - \Delta a_z z_C = \bar{\beta}_{11} b_1 e_z (t - \tau_1) \tag{20}$$

$$m_C \ddot{z}_C = 2k_{F1}q_{zC} + d_{zC}, \qquad T_{C1}\dot{q}_{zC} + q_{zC} - a_{zC} z_C - \Delta a_z z = \bar{\beta}_{11} b_1 e_{zC} (t - \tau_1) \tag{21}$$

where

$$m_C = \frac{J}{L^2}, \qquad d_{zC} = \frac{M(d_z)}{L}$$

$$a_z = \frac{1}{2}(a_{10} + c_{kFz} a_{20}), \qquad a_{zC} = \frac{1}{2}\left[\left(\frac{L_1}{L}\right)^2 a_{10} + \left(\frac{L_2}{L}\right)^2 c_{kFz} a_{20}\right]$$

$$\Delta a_z = \frac{1}{2}\left[\frac{L_1}{L} a_{10} - \frac{L_2}{L} c_{kFz} a_{20}\right]$$

There are no interacting terms $\Delta a_z z_C$ and $\Delta a_z z$ in eqs. (20) and (21) in the case of a symmetric bearing system or in a supporting condition (ref. 6); we may neglect them in many cases. Omitting them, we design the control systems of the two motions with the control variables e_z and e_{zC}. To realize the designed control actions, from eq. (19) we assign the actual control inputs into the electromagnets as follows:

$$e_1 = \frac{L_2}{L} e_z + e_{zC}, \qquad e_2 = \frac{1}{c_{ez}}\left(\frac{L_1}{L} e_z - e_{zC}\right) \tag{22}$$

The similar equations of the horizontal direction are given as a special case of the above results.

EXPERIMENTS

Experimental Setup

Figure 3 shows the mechanical part of the experimental set up of the symmetric radial bearings supporting a symmetric rotor in the horizontal direction. The stator and rotor cores are made of silicon steel strips of 0.2mm thickness. The four stator rings of the two bearings are of equal dimensions. The pole legs are of the same size in the horizontal direction and on the lower side in the vertical direction. The pole legs on the upper side are 25% wider than the others, to give a larger permanent magnet flux to suspend the deadweight of the rotor. A sheet of paper was pasted on the pole-leg faces to prevent direct contact with the rotor. The turns in the electromagnet coils are all the same. The connecting segments may be made of solid iron, but we used silicon steel strips, for convenience.

The rotor cores in the shape of a ring have outer and inner diameters of 50mm and 19mm, respectively, and are guided on a shaft of aluminum. The permanent magnet made of neodymium has an outer diameter of 39mm, an inner diameter of 19mm and a thickness of 7mm. Two spacer rings of aluminum are used to adjust the bias flux. We adjusted its density to be about 0.45T in the nominal working airgap length to suspend the deadweight of the rotor without electromagnet bias current. Four displacement sensors of the eddy current type are used to detect the radial displacement of the rotor. The rotation is given by compressed air blown onto teeth in the middle of the shaft. The primary specifications are given in **Table 1.**

The rotor-position control systems are constructed to realize the decoupling control systems, based on eqs. (20)- (22) with parallel analog PID compensators. The input voltage into the power amplifiers is limited to a value of about 4V to give the maximum coil current of 2.4A that is nearly equal to the

value of current cancelling the bias flux with the nominal working airgap. The gains of the compensators were adjusted experimentally with a sinusoidal input of amplitude 1V in a similar way to the measurement of frequency response shown later. The selected gains gave a phase margin of 32 deg. at 180 Hz and a gain margin of 10dB at about 510Hz in the vertical translatory control system, and 44 deg. at about 200Hz and 9dB at 590Hz, respectively, in the vertical conical control system. We gave similar margins to the horizontal control system.

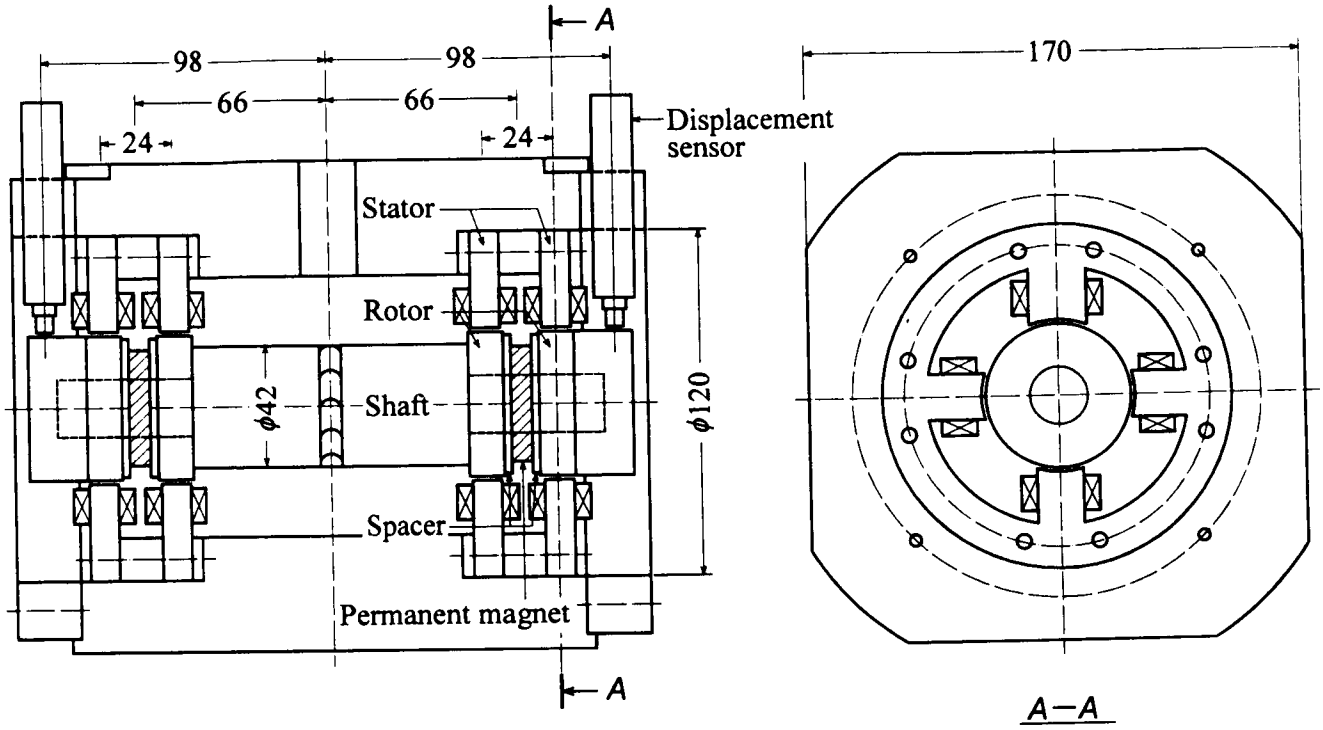

Figure 3. Experimental setup of active magnetic bearings biased with permanent magnets on the rotor.

Frequency Responses of Rotor Motion

In the non-rotating state, we measured frequency responses of the rotor displacement to a non-biasing sinusoidal signal superimposed on the control input of the decoupled control systems: for example, in eq. (20)

$$e_z = \bar{e}_z + e_0 \tag{23}$$

where $\bar{e}_z$ is the control input of the translatory motion and e_0 is the sinusoidal input. **Figure 4** shows by the solid lines the response of the vertical translatory control system with an input amplitude of 1V. The maximum gain at about 35Hz corresponds to a displacement amplitude of 0.12mm. With input amplitude 2V, we obtained a gain response that is very close to this response but slightly lower around the frequency giving the maximum gain (the maximum amplitude is 0.21mm).

Figure 5 shows the response in the vertical conical control system with an amplitude of 1V; the maximum displacement amplitude is estimated to be 0.13mm at about 25Hz. We had a very close response to the amplitude of 1.5V with the maximum amplitude of 0.18mm.

Table 1 Specifications and Data of Experimental Setup

Rotor : Mass	$m = 1.35$	kg
Outer diameter	$D = 50.0\times10^{-3}$	m
Moment of inertia of conical motion	$J = 56.7\times10^{-4}$	kgm^2
Polar moment of inertia	$J_p = 3.94\times10^{-4}$	kgm^2
Distance between bearing centers	$2L_1 = 132\times10^{-3}$	m
Distance between two gap sensors	$2L_{m1} = 196\times10^{-3}$	m
Stator		
Cross-sectional area of pole leg : Upper	$A_{hi2} = 2.0\times10^{-4}$	m^2
Others	$A_{hij} = 1.6\times10^{-4}$	m^2
Working airgap length	$l_{ij0} = 0.6\times10^{-3}$	m
Displacement sensor gain : Translatory	$k_{ST} = 5.0\times10^{3}$	V/m
Conical	$k_{SC} = 7.4\times10^{3}$	V/m
Permanent magnet : Bias flux density in airgap	$B_0 = 0.441$	T
Equivalent coil current	$Q_{Bij} = 2.14$	A
Recoil permeability	$\mu_r = 1.0$	
Electromagnet : Turns of coil	$N_{ij} = 100$	
Gain of power amplifier	$b_1 = 0.61$	A/V
Relative permeability of magnet core	$\mu_S = 5{,}000$	
Calculated data		
Bias coil current : Vertical	$I_{10} = -0.01$	A
Horizontal	$I_{30} = 0$	A
Bias force : Lower	$2F_{110} = 24.6$	N
(Single bearing) Upper	$2F_{120} = 31.2$	N
Horizontal	$2F_{130} = 24.8$	N
Force constant : Vertical	$k_{F1} = 46.0$	N/A
(Single bearing) Horizontal	$k_{F3} = 46.2$	N/A
Instability constant : Vertical	$a_z = a_{zC} = 3{,}960$	A/m
Horizontal	$a_y = a_{yC} = 3{,}510$	A/m
Constant	$\bar{\beta}_{11} = 1.12$	A/V
Time constants : Time constant of coil current	$T_{C1} = 0.10\times10^{-3}$	s
Dead time of power amplifier	$\tau_1 = 0.02\times10^{-3}$	s

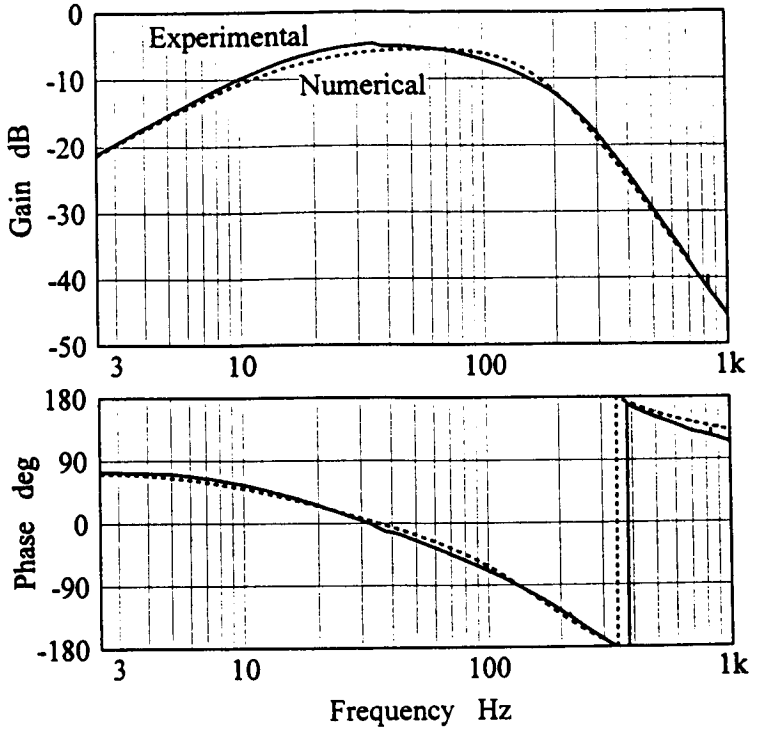

Figure 4. Frequency response of translatory rotor motion.

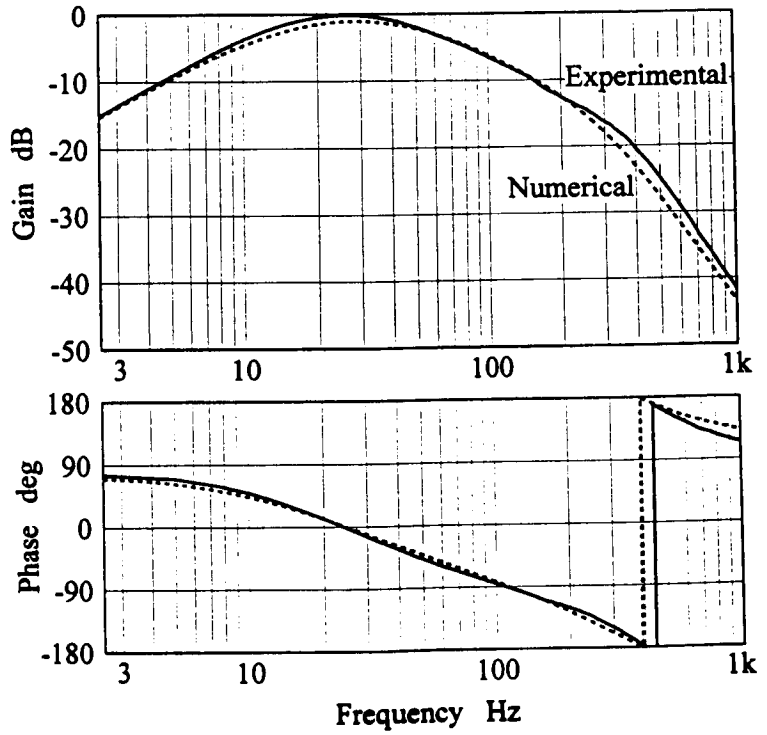

Figure 5. Frequency response of conical rotor motion.

Numerical Results of Frequency Responses

The permanent-magnet flux density was 0.441T on average in the measurement with the nominal airgap. This value is used to calculate the equivalent bias current of eq. (3) and the bias force of eq. (8); we take a value of 5,000 for the relative permeability of the magnet cores. Then, the constants in eqs. (20) and (21) are calculated as in Table 1 when we neglect the electromagnetic flux axially passing through the rotor and the connecting segments ($R_R + R_B = \infty$). In this case, statically, the electromagnetic flux bypassing the horizontal pole legs is calculated to be about 12% of the flux of the vertical lower pole leg, i.e., the flux on the upper side is about 12% more than that on the lower side. The measured values were about 7% and 15%, respectively (the difference of 8% seems to have taken other paths). The time constants of the electromagnet system in eq. (5) are identified from the frequency characteristics of the coil current with the fixed nominal-airgap. We obtained a very good approximation to the characteristics whose values are shown in the lowest part of Table 1.

The numerical frequency responses of eq. (20) with the input of eq. (23) and eq. (21) with the similar input are drawn by the broken lines in Figs. 4 and 5. The gain response of the translatory motion is a little different from the experimental result in the frequencies of about 10Hz to 200Hz, but very close above 200Hz. About the conical motion, there is a little difference under 50Hz and a larger difference above 200Hz. We presently have no idea about these differences.

From the numerical analysis, we see that the gain characteristics depend mainly on the gains of the compensator, in particular, the integral action's gain, in lower frequencies, on the instability constant, a_z or a_{zC}, in the intermediate frequencies, and on the force constant, k_{Fi}, in higher frequencies. We can obtain the gains of the compensator, so that we have good agreement in the lower frequencies.

Transient Motion to Impact

Figure 6 shows the translatory rotor motion and the actual control input into the power amplifier for a vertical impulsive force that directly acts at the center of the shaft in the non-rotating state. The maximum displacement of about 0.4mm is about 70% of the nominal working-airgap length; the rotor was regulated in about 20ms. The input into the power amplifier was attenuated by a factor of 0.69, and the maximum input was designed to be about 2.8V(4 × 0.69). The constant b_1 in Table 1 is given by the series attenuation of this factor and the static gain of the coil current to the input, 0.89.

Decay of Rotation and Whirling of Rotor

We ran the rotor up to 25,000rpm. **Figure 7** gives a decay of rotation due to magnetic braking with air friction without driving. From 25,000rpm the rotation decreases to 1,000rpm in about 5.4min and to zero in about 6.3min. The decay is approximated by the curve given by the equation

$$\dot{\omega} + 3.5 \times 10^{-3}\omega + 2.5 \times 10^{-6}\omega^2 = -1.85, \quad \omega : \text{rad/s} \tag{24}$$

We observed the whirling of the rotor together with the rotation decay. The amplitudes in the vertical and horizontal directions are shown in **Fig. 8.** The whirling is larger in the horizontal direction than in the vertical direction above 16,000rpm, but smaller below it. We had not checked the rotor balancing and had seen that there was an installation error of the sensor target rings for displacement sensing. We suppose these are reasons why the whirling is relatively large.

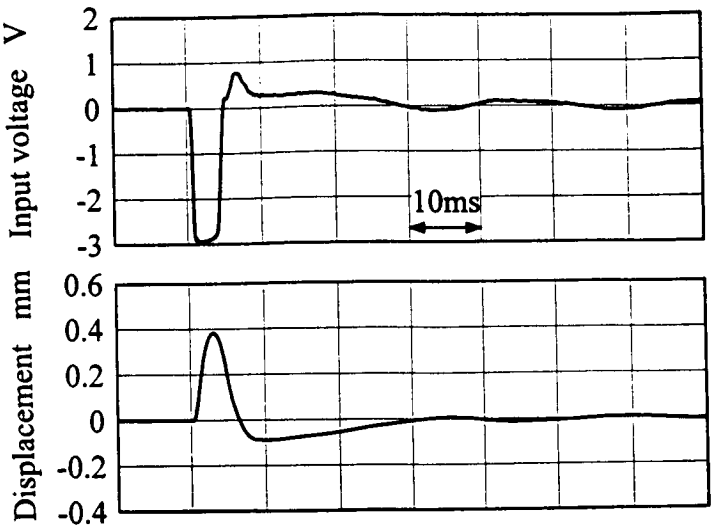

Figure 6. Transient motion to impact.

CONCLUSIONS

We considered the characteristics of the radial magnetic bearings biased with permanent magnets arranged on the rotor. First, we presented a simple linearized model of control force that is similar to that of the all electromagnetic design. Second, in the non-rotating state, we measured the frequency responses of the rotor positioning control and compared those with the numerical results to check the validity of the simple model. We also gave the transient displacement of the rotor for impact directly acting on the rotor. Last, we examined the decay of the rotation mainly due to magnetic braking with the whirling of the rotor. The data obtained show the characteristics similar to those of the all electromagnetic design.

The construction of electromagnets with opposing coils in a series connection gives a property that the time constant of the electromagnet system does not vary so much with working airgap length. This construction may be adopted in the all electromagnetic case as in ref. 7, for example, but may be uncommon to these applications at present. While this construction may lead to the interactions of the magnetic systems, we have not encountered a serious problem in our experiments.

We thank the Nippon Steel Corp. for supplying us the silicon steel strips. We also acknowledge Mr. Fujino, S. for machining the experimental setup, and Undergraduate students Watanabe, T. and Yanai, N. for help in assembling the setup and in the experiment.

REFERENCES

1. *NASA Tech. Brief*, B74-10131, Sept. 1974.

2. *Design News*, 6-11-90, p.156.

3. Allaire, P. E.; *et al*.:: Permanent Magnet Biased Magnetic Bearings-Design, Construction, and Testing, *Proc. 2nd Inter. Sympo. Magnetic Bearings*, pp.175-182, Tokyo, June 1990.

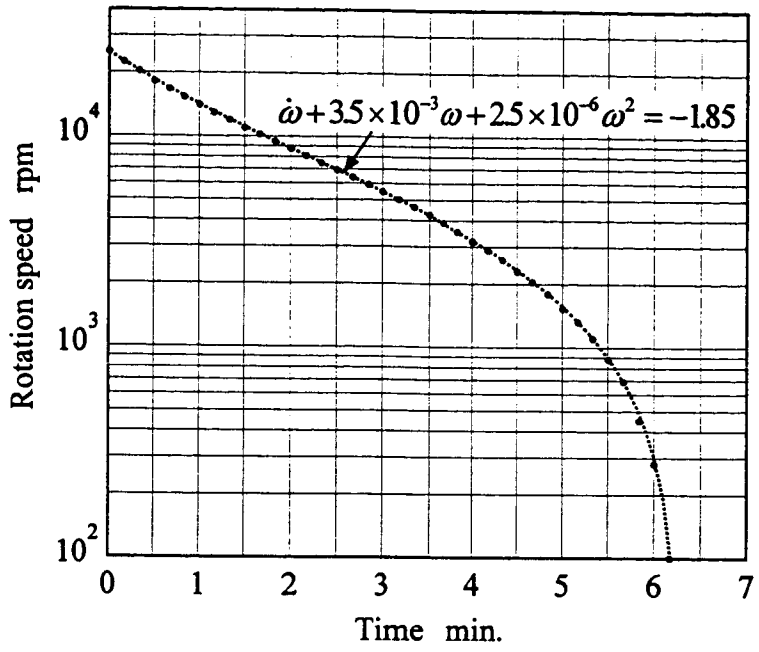

Figure 7. Decay of rotation.

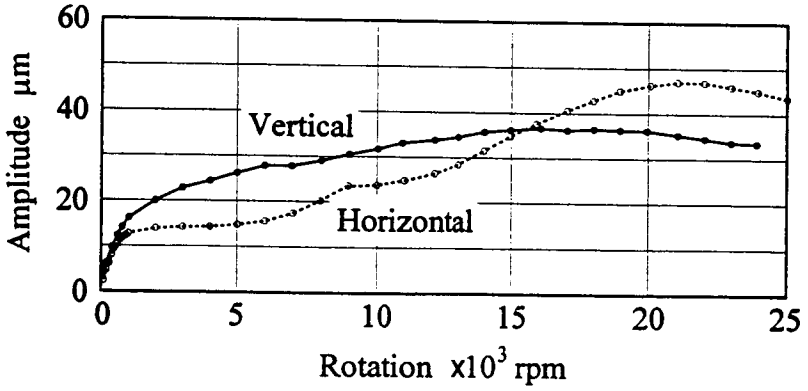

Figure 8. Amplitude of whirling of rotor.

4. Fukata, S.; and Yutani, K.: Dynamics of Permanent-Magnet Biased Active Magnetic Bearings, *Proc. 3rd Inter. Sympo. Magnetic Suspension and Technology,* Part 2, pp. 721-736, July 1996.

5. Fukata, S.; and Yutani, K.: Analysis of Magnetic systems of Magnetic Bearings Biased with Permanent Magnets, *Memoirs of Fac. Engg., Kyushu Univ.*, Vol.57, No.1, pp.17-35, March, 1997.

6. Fukata, S.; and Kouya, T.: Control Systems of Active Magnetic Bearings Based on Decoupling of the Motion of Rigid Rotor, *Technology Report of Kyushu Univ.* (in Japanese), Vol. 60, No. 2, pp.185-191, 1987.

7. Ozeki, et al., Magnetic Bearings Supporting Spindles, *Bearing Engineer* (in Japanese), No. 51, p.55, 1985.